# Normal form of synchronization and resonance between vorticity waves in shear flow instability

Eyal Heifetz

*Department of Geophysics, Porter School of the Environment and Earth Sciences, Tel Aviv University, Tel Aviv 69978, Israel*

Anirban Guha[*]

*Institute of Coastal Research, Helmholtz-Zentrum Geesthacht, Geesthacht 21502, Germany*

A minimal model of linearized two-dimensional shear instabilities can be formulated in terms of an action-at-a-distance, phase-locking resonance between two vorticity waves, which propagate counter to their local mean flow as well as counter to each other. Here we analyze the prototype of this interaction as an autonomous, nonlinear dynamical system. The wave interaction equations can be written in a generalized Hamiltonian action-angle form. The pseudoenergy serves as the Hamiltonian of the system, the action coordinates are the contribution of the vorticity waves to the wave action, and the angles are the phases of the vorticity waves. The term "generalized action angle" emphasizes that the action of each wave is generally time dependent, which allows instability. The synchronization mechanism between the wave phases depends on the cosine of their relative phase, rather than the sine as in the Kuramoto model. The unstable normal modes of the linearized dynamics correspond to the stable fixed points of the dynamical system and vice versa. Furthermore, the normal form of the wave interaction dynamics reveals a new type of inhomogeneous bifurcation: annihilation of a stable and an unstable star node yields the emergence of two neutral center fixed points of opposite circulation.

## I. INTRODUCTION

In their seminal paper, Hoskins *et al.* [1] presented a heuristic minimal model for barotropic shear instability based on the interaction at a distance between two counterpropagating Rossby waves. This model has been formulated mathematically by Heifetz *et al.* [2] for the simple barotropic model of Rayleigh [3] and by Davies and Bishop [4] for the simple baroclinic model of Eady [5]. Later Methven *et al.* [6] showed that this minimal model catches, surprisingly well, the essence of the instability of realistic atmospheric jets with complex baroclinic-barotropic structures. Harnik *et al.* [7] then showed that the concept of resonance action at a distance in shear flows is not exclusive to Rossby wave instability, but it can be applied to gravity waves in stratified shear flows; cf. Guha and Lawrence [8] and the thorough review by Carpenter *et al.* [9]. Following that, Biancofiore *et al.* [10] applied the model to include interfacial capillary wave instability between immiscible sheared fluid layers and Heifetz *et al.* [11] to Alfvén waves in magnetohydrodynamic shear flows.

Despite its importance, and to the best of our knowledge, this minimal model has never been analyzed as a stand-alone dynamical system, which is the purpose of this paper. We aim to focus on its normal form, type of bifurcations, the synchronization mechanism, and the relation of this model to other generic nonlinear systems such as the Kuramoto model

[12] and the bifurcations described by the complex Landau equation [13].

The schematic picture of the interaction in its simplest form can be drawn as follows. Consider a two-dimensional (2D) shear flow profile, plotted in Fig. 1, in the $(x, y)$ plane. The mean flow $U(y)$ is pointing only in the $x$ direction, but its speed varies with $y$. Furthermore, $U(y)$ is positive in region I and negative in region II. The vorticity, $\Omega$, for a 2D flow is a scalar, and for this shear flow profile, $\Omega(y) = -dU/dy$ is nonpositive everywhere. Its cross-stream derivative however, $d\Omega/dy = -d^2U/dy^2$, is positive in region I and negative in region II. Such flow satisfies the two celebrated necessary conditions for shear instability of Rayleigh [3] and Fjørtoft [14]. The Rayleigh inflection point criterion requires that the mean vorticity's cross-stream derivative changes sign within the shear region, whereas the Fjørtoft condition has an additional requirement: the signs of the cross-stream vorticity derivative and the mean flow should be positively correlated. In our case, both fields are positive in region I and negative in region II, thereby satisfying Fjørtoft's criterion in addition to Rayleigh's criterion.

The Rayleigh and Fjørtoft conditions were derived originally for normal mode instability and only in 1985 [1] were related to the more general constants of motion in linearized dynamics of pseudomomentum (or equivalently wave action, for monochromatic waves) and pseudoenergy, respectively. In that seminal paper, the authors provided as well a minimal model to rationalize these conditions, as is illustrated below. In a 2D inviscid, incompressible flow, a fluid element with the velocity field $\mathbf{u} = (u, v)$ materially conserves its vorticity, $\tilde{q} = \partial v/\partial x - \partial u/\partial y$, as it moves. Since in region I the

---

[*]anirbanguha.ubc@gmail.com; present address: School of Science and Engineering, University of Dundee, Dundee DD1 4HN, United Kingdom.
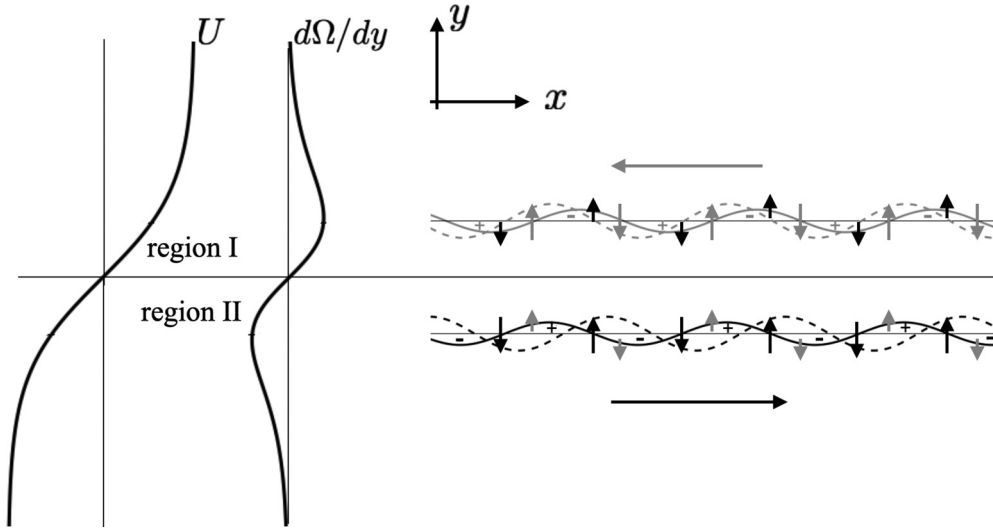
FIG. 1. Schematic of interacting vorticity waves in a shear flow. A hyperbolic tangent shear layer and the corresponding vorticity gradient profile are shown on the left-hand side. On the right-hand side, the cross-stream displacement, the associated cross-stream velocity, and the associated sign of vorticity for each wave are shown and represented by the same color. The position of each undulating material line after a short time interval is shown by dashed line. Interaction leads to an additional cross-stream velocity (shown by a different color). Note that cross-steam velocities due to undulations of the other material line are weaker (represented by shorter arrows) than those due to the self-induced vorticity anomalies. The horizontal arrow associated with a wave indicates the intrinsic wave propagation direction. Both waves are counterpropagating, i.e., moving opposite to the background velocity at that location.

cross-stream derivative of the mean vorticity is positive, a fluid element that is displaced southward (in the negative $y$ direction) conserves its relatively high vorticity and consequently develops a positive vorticity anomaly, $q$, which induces a counterclockwise circulation. Similarly, a fluid element that is displaced northward develops a negative vorticity anomaly with clockwise circulation. Thus, an undulated sinusoidal material line in region I (indicated by the gray solid line in Fig. 1) will tend to propagate to the west (in the negative $x$ direction, the dashed gray line), counter to the mean flow $U$, because the induced cross-stream velocity will shift fresh vorticity anomalies to the left of the existing ones.

Applying the same logic to region II, an undulated sinusoidal material line here will propagate to the east (black solid and dashed lines in Fig. 1), counter as well to the mean flow there. These waves, denoted as shear Rossby waves, are the building blocks of the minimal model. The sign of the cross-stream mean vorticity gradient determines the direction of their intrinsic phase speed. Therefore, when the Rayleigh's criterion is satisfied, the waves propagate counter to each other, and when the Fjørtoft condition is satisfied as well, the waves also propagate counter to their local mean flow. Consequently, despite the mean shear, and even in the absence of interaction between the waves, the difference between the waves' phase speeds is relatively small.

The second essential ingredient in this minimal model is the interaction at a distance between those building blocks. While the waves' vorticity fields are localized, the velocity field attributed to each vorticity field is nonlocal by nature and decays away from each vorticity wave. Consequently, the two waves can interact at a distance by inducing on each other their individual cross-stream velocities. If the two waves' vorticity fields are in phase [Fig. 2(a)], their cross-stream velocity will be in phase as well. Therefore, the induced velocity

of one wave on the other will "help" the latter to translate its displacement faster, and as a result, each wave will be propagating faster counter to its mean flow. In contrast, if the vorticity of the waves are in antiphase [Fig. 2(b)], the waves will hinder each other's counterpropagation rate. If the upper wave's vorticity lags the lower one by a quarter of a wavelength (so that the waves are $\pi/2$ out of phase), the far-field velocity induced by each wave will not affect the propagation rate but will amplify the waves' displacements. As each wave's displacement amplitude is tied to its vorticity, an increase in the vorticity amplitude of one wave will lead to an amplification of the vorticity amplitude of the other wave. Therefore, this scenario describes a mutual instantaneous amplification at a distance [Fig. 2(c)]. In contrast, if it is the lower wave's vorticity which is lagging the upper one by a quarter of a wavelength, the waves will mutually decay each other's amplitudes [Fig. 2(d)]. Generally, any setup of phase difference between the two waves yields mutual interactions that affect both the waves' amplitudes and the waves' propagation rates [Fig. 2(e)]. Figure 1 demonstrates a configuration where the waves amplify each other's amplitude but hinder each other's counterpropagation rate.

The wave interaction picture described above can be translated into a generic set of equations constructing the minimal model. Denote the vorticity waves' anomaly in the two regions as $q_{1,2}(t)$, and writing them in terms of their amplitudes and phases $q_{1,2} = Q_{1,2} e^{i \epsilon_{1,2}}$, we follow Ref. [15] to obtain

$$\dot{Q}_1 = \sigma_1 Q_2 \sin \epsilon, \quad \dot{Q}_2 = \sigma_2 Q_1 \sin \epsilon, \tag{1a}$$

$$\dot{\epsilon}_1 = -\hat{\omega}_1 + \sigma_1 \frac{Q_2}{Q_1} \cos \epsilon, \quad \dot{\epsilon}_2 = -\hat{\omega}_2 - \sigma_2 \frac{Q_1}{Q_2} \cos \epsilon. \tag{1b}$$

Consider the first equation set (1a), which relates to the inner circle of Fig. 2(e) and describes the instantaneous growth
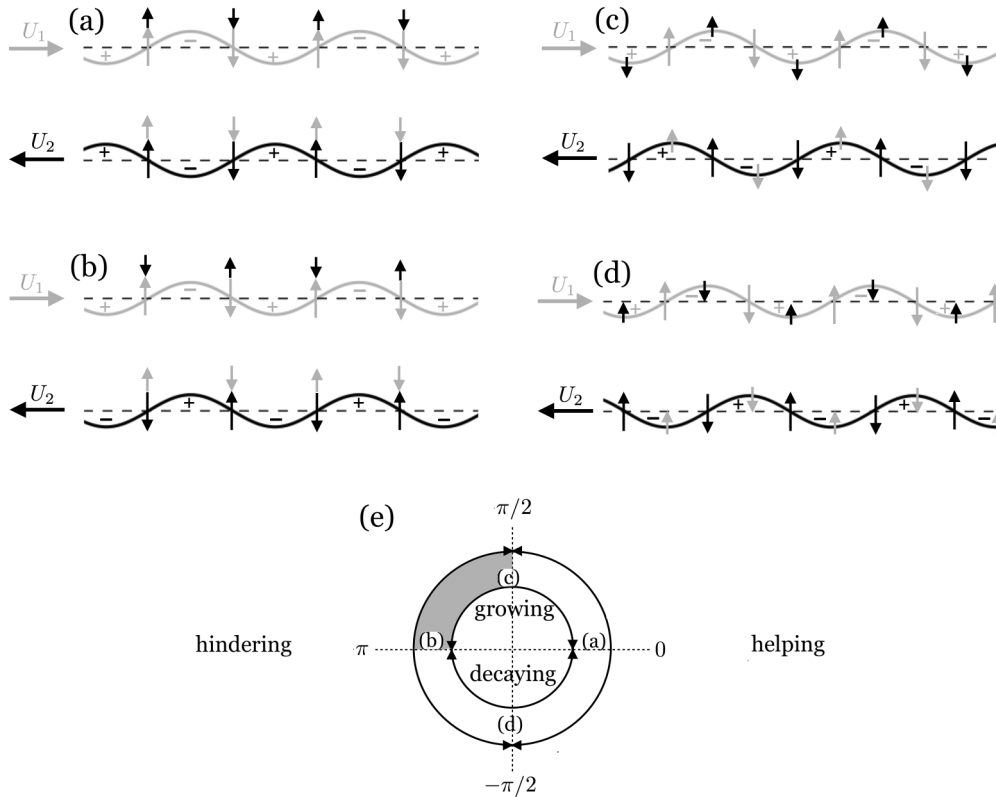
FIG. 2. Schematic description of the linear interactions between counterpropagating vorticity waves. The waves depict interfacial displacement, while the horizontal and vertical arrows, respectively, denote streamwise (background) and cross-stream velocities. Note that cross-steam velocities due to undulations of the other material line are weaker (represented by shorter arrows) than those due to the self-induced vorticity anomalies. (a) Fully helping, (b) fully hindering, (c) fully growing, and (d) fully decaying configurations. (e) Depending on the phase difference $\epsilon$ between the vorticity perturbations at the upper and lower undulating material lines, different kinds of linear interactions can be expected, as shown by the "concentric circles." The locations where the configurations (a)–(d) occur have been marked. The configuration given in Fig. 1 lies in the second quadrant (shaded in gray), which is the "growing-hindering configuration."

or decay of the wave amplitudes due to the interaction at a distance. The waves' relative phase is $\epsilon \equiv \epsilon_1 - \epsilon_2$, while the interaction at a distance coefficients, $\sigma_{1,2}$, depend on the details of the problem. Note that $\sigma_1$ is determined by the evanescent structure of the cross-stream velocity of wave 2, the effective distance between the two waves and the cross-stream mean vorticity gradient in region I (where equivalent arguments are implied for $\sigma_2$). It indeed indicates that $\epsilon = \pi/2$ [Fig. 2(c)] is the optimal phase for mutual instantaneous amplification. Equation set (1b) relates to the outer circle of Fig. 2(e). The waves' frequencies, $\hat{\omega}_{1,2}$, in the absence of interaction includes both the effects of advection by the mean flow, $U_{1,2}$ (which provides the Doppler shift), and the counterpropagation rate (which is the intrinsic frequency). The frequency of each wave can be either positive or negative. Positive values of $\hat{\omega}_{1,2} > 0$, indicate eastward wave propagation (in the positive $x$ direction) in the absence of interaction, where the minus sign in front of them, at the right-hand side of (1b), is because the waves' phases increase when they propagate westward. Thus, when the waves' vorticity fields are in phase [$\cos \epsilon = 1$; see Fig. 2(a)], the waves help each other to counterpropagate in agreement with the plus and minus signs in the last terms of Eq. (1b) [16]. The same logic can be applied for $\epsilon = \pi$, Fig. 2(b), where the waves hinder each other's propagation rate.

It is worth noting that although the system (1) is composed of inhomogeneous *nonlinear* ordinary differential equations, it describes the *linearized dynamics* of small perturbations in shear flows. This is, to some extent, analogous to the nonlinear description of the small amplitude dynamics of two coupled pendulums. This toy model should be taken more as a conceptual model rather than an exact one and is related only to the onset phase of the instability. Obviously for finite (even small) amplitudes, each wave in each of the regions will feel the shear within its own region and consequently will lose its coherency. Nevertheless, it is somewhat surprising how reasonably well this minimal model catches the essence of the instability dynamics in some circumstances. In the Appendix we compare the exact solution of a piecewise linear shear profile approximation (also known as the Rayleigh problem [3]) to the hyperbolic tangent mixing layer profile plotted in Fig. 1. For the Rayleigh setup, equation set (1) is an exact description of the discrete spectrum dynamics [2]. It is surprising how similar the dispersion relations of the two problems are, and how similar are the structures of their most unstable modes. Even more surprising, when the fully nonlinear dynamics of equilibrated baroclinic [6] and barotropic [17] jets were analyzed, the power spectrum evolution partly obeys the dynamics of equation set (1). Furthermore, Ref. [15] showed how generally the discrete spectrum of a linearized dynamics,

conserving potential vorticity, can be mapped into equation set (1), albeit the vorticity waves are not generally localized if the shear profile is composed of a series of concave and convex sections (see, e.g., Fig. 9 below).

Note also that the Rossby wave mechanism is only one possibility to obtain counterpropagating vorticity waves. Waves whose vorticity and cross-stream displacement fields are in (anti) phase will propagate to the (west) east, relative to the mean flow, as the cross-stream velocity will shift the displacement accordingly. If a different restoring force translates the vorticity in concert, then the essence of the dynamics of (1) is still applicable. Examples of such other vorticity wave dynamics are gravity [7] and capillary [10] waves in stratified shear flows and Alfvén [11] waves in magnetohydrodynamical shear systems.

The organization of the paper is as follows. In Sec. II we derive its general properties, and then in Sec. III we analyze the dynamics in detail with relation to the physical interaction mechanism described in the introduction. In Sec. IV we implement these results to the concrete example of the Rayleigh piecewise linear shear profile, and then in Sec. V we generalize the two-wave interactions of Eq. (1) to the case of multiple-wave interactions. We close by concluding our results in Sec. VI.

## II. GENERAL DYNAMICAL PROPERTIES

### A. Generalized canonical action-angle formulation

It is straightforward to verify that the system (1) conserves the following two constants of motion:

$$\mathcal{H} = -\hat{\omega}_1 \frac{Q_1^2}{2\sigma_1} + \hat{\omega}_2 \frac{Q_2^2}{2\sigma_2} + Q_1 Q_2 \cos\epsilon$$

$$= -(\hat{\omega}_1 \mathcal{A}_1 + \hat{\omega}_2 \mathcal{A}_2) - 2i\sigma\sqrt{\mathcal{A}_1 \mathcal{A}_2}\cos\epsilon, \quad (2a)$$

$$\mathcal{A} = \frac{Q_1^2}{2\sigma_1} - \frac{Q_2^2}{2\sigma_2} = \mathcal{A}_1 + \mathcal{A}_2, \quad (2b)$$

where $\sigma \equiv \sqrt{\sigma_1 \sigma_2}$ is the geometric mean of the interaction coefficients. The first conserved quantity is denoted as the pseudoenergy of the system, and the second is its action, which is also proportional to the psuedomomentum [15,18]. The term "generalized" is used here because, as opposed to the classical action-angle formulation, the actions associated with each wave (each degree of freedom), $\mathcal{A}_1 = [Q^2/(2\sigma)]_1$ and $\mathcal{A}_2 = -[Q^2/(2\sigma)]_2$, are not conserved individually. It is also straightforward to verify that

$$\mathcal{H} = \mathcal{A}_1 \dot{\epsilon}_1 + \mathcal{A}_2 \dot{\epsilon}_2.$$

Therefore, Eqs. (1a)–(1b) can be rewritten in a canonical generalized action-angle form, in which $\mathcal{H}$ serves as the Hamiltonian:

$$\dot{\mathcal{A}}_1 = -2i\sigma\sqrt{\mathcal{A}_1 \mathcal{A}_2}\sin\epsilon = -\frac{\partial \mathcal{H}}{\partial \epsilon_1},$$

$$\dot{\mathcal{A}}_2 = 2i\sigma\sqrt{\mathcal{A}_1 \mathcal{A}_2}\sin\epsilon = -\frac{\partial \mathcal{H}}{\partial \epsilon_2}, \quad (3a)$$

$$\dot{\epsilon}_1 = -\hat{\omega}_1 - i\sigma\sqrt{\frac{\mathcal{A}_2}{\mathcal{A}_1}}\cos\epsilon = \frac{\partial \mathcal{H}}{\partial \mathcal{A}_1},$$

$$\dot{\epsilon}_2 = -\hat{\omega}_2 - i\sigma\sqrt{\frac{\mathcal{A}_1}{\mathcal{A}_2}}\cos\epsilon = \frac{\partial \mathcal{H}}{\partial \mathcal{A}_2}. \quad (3b)$$

To avoid confusion, note that Eqs. (2)–(3) comprise only real terms because $\mathcal{A}_2$ is negative definite; here we took its positive root $\sqrt{\mathcal{A}_2} = i[Q/\sqrt{2\sigma}]_2$.

### B. The complex normal form

The nonlinear, real, inhomogeneous set of Eqs. (1a)–(1b) results from linearization of the material conservation of vorticity equations in the two regions. The latter yields a set of the following two linear, complex, homogeneous equations [see Eqs. (11)–(12) of Ref. [15] and Eqs. (4.1)–(4.2) of Ref. [8]]:

$$\dot{q}_1 = -i\hat{\omega}_1 q_1 + i\sigma_1 q_2, \quad (4a)$$

$$\dot{q}_2 = -i\hat{\omega}_2 q_2 - i\sigma_2 q_1. \quad (4b)$$

Define the complex variable:

$$\mathcal{Z} \equiv \sqrt{\frac{\sigma_2}{\sigma_1}} \frac{q_1}{q_2} \equiv \chi e^{i\epsilon}, \quad (5)$$

where $\chi = \sqrt{\sigma_2/\sigma_1}(Q_1/Q_2)$ is a scaled ratio of the wave amplitudes. Hence Eqs. (4a)–(4b) can be then written in the compact complex form

$$\dot{\mathcal{Z}} = i\sigma\left[\mathcal{Z}\left(\mathcal{Z} - \frac{\hat{\omega}}{\sigma}\right) + 1\right], \quad (6)$$

where $\hat{\omega} \equiv \hat{\omega}_1 - \hat{\omega}_2$. Defining the control parameter $\mu \equiv \hat{\omega}/\sigma$, and using a scaled time $\tau \equiv \sigma t$, Eq. (6) can be expressed as the following normal form:

$$\frac{d\mathcal{Z}}{d\tau} = i[\mathcal{Z}(\mathcal{Z} - \mu) + 1]. \quad (7)$$

The normal form is complex because it describes the evolution of both the waves' amplitudes and phases. It is inhomogenous since the mean flow acts as an external forcing. Furthermore, the essence of the system dynamics is an interaction between waves with different intrinsic frequencies. Thus, the dynamics is controlled by a single parameter, which is the ratio between the frequency difference of the two waves and the mean interaction coefficient.

### C. Relations between fixed points and normal modes

The complex fixed points of Eq. (7) are obtained when the waves' (scaled) amplitude ratio $\chi^*$ and their relative phase $\epsilon^*$ remain fixed (where the asterisk denotes the values at the fixed points):

$$\frac{d\mathcal{Z}}{d\tau} = e^{i\epsilon}\left[\frac{d\chi}{d\tau} + i\chi\frac{d\epsilon}{d\tau}\right] = 0. \quad (8)$$

We also note that these fixed points are the normal modes of the equivalent linear system Eq. (4). To show this we write the latter in a matrix form:

$$\dot{\mathbf{q}} = \mathbf{A}\mathbf{q}; \quad \mathbf{q} = \begin{bmatrix} q_1 \\ q_2 \end{bmatrix},$$

$$\mathbf{A} = -i\begin{bmatrix} \hat{\omega}_1 & -\sigma_1 \\ \sigma_2 & \hat{\omega}_2 \end{bmatrix} \Rightarrow \mathbf{q} = \sum_{j=1}^{2} a_j \mathbf{p}_j e^{\lambda_j^{NM}t}, \quad (9)$$
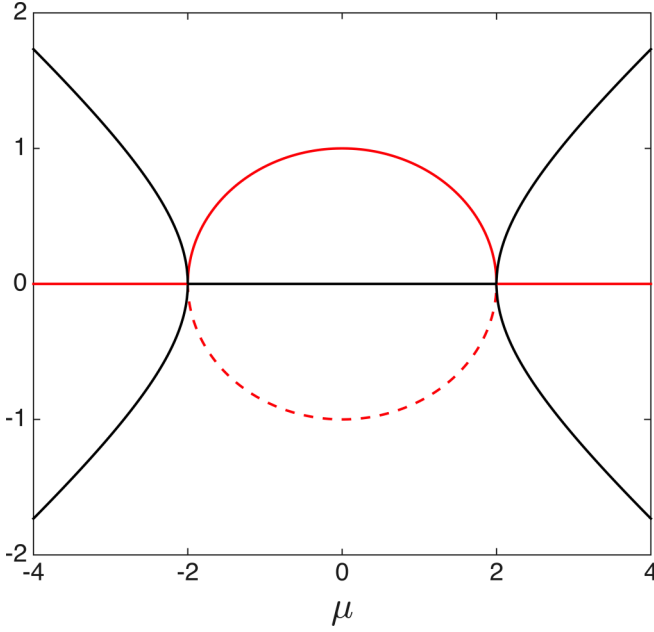
FIG. 3. Bifurcation diagram. Black line denotes $\lambda_i^{NM}$, and red line denotes $\lambda_r^{NM}$. The unstable normal modes ($\lambda_r^{NM} > 0$) compose the branch of stable fixed points (marked by the solid red line) of the dynamical system Eq. (7), whereas the stable modes ($\lambda_r^{NM} < 0$) compose the unstable branch (marked by the dashed red line).

where $a_j$ are constants, and $\mathbf{p}_j$ and $\lambda_j^{NM}$ are, respectively, the complex eigenvectors and eigenvalues of $\mathbf{A}$. Then if we denote

$$\mathbf{p}_j = \begin{bmatrix} P_1 e^{i\phi_1} \\ P_2 e^{i\phi_2} \end{bmatrix}_j, \quad \phi \equiv \phi_1 - \phi_2, \quad \lambda^{NM} = \lambda_r^{NM} + i\lambda_i^{NM},$$

$$(10)$$

the $j$th normal mode solution can be written as

$$\mathbf{q} = \begin{bmatrix} Q_1 e^{i\epsilon_1} \\ Q_2 e^{i\epsilon_2} \end{bmatrix} = \begin{bmatrix} (P_1 e^{\lambda_r^{NM} t}) e^{i(\phi_1 + \lambda_i^{NM} t)} \\ (P_2 e^{\lambda_r^{NM} t}) e^{i(\phi_2 + \lambda_i^{NM} t)} \end{bmatrix}_j. \quad (11)$$

Therefore, $\chi^* = \sqrt{\sigma_2/\sigma_1}(Q_1/Q_2)_j^* = \sqrt{\sigma_2/\sigma_1}(P_1/P_2)_j = $ const$_1$ and $\epsilon_j^* = (\epsilon_1 - \epsilon_2)_j = \phi_j = $ const$_2$. To simplify the analysis we hereafter refer to the motion in the frame of reference of the mean frequency (rather, phase speed) in the absence of interaction, i.e., $\overline{\omega} = (\hat{\omega}_1 + \hat{\omega}_2)/2$. There the eigenvalues of $\mathbf{A}$ (normalized by $\sigma$) satisfy

$$\lambda_{1,2}^{NM} = \pm\sqrt{1 - \left(\frac{\mu}{2}\right)^2}. \quad (12)$$

Note that the condition of constant wave amplitude ratio applies for normal modes with either positive, negative, or zero growth rate ($\lambda_r^{NM}$), and the phase-locking condition implies that the waves are moving in concert with the same frequency ($-\lambda_i^{NM}$), which as well can be either positive, negative, or zero. The dependence of eigenvalues on the bifurcation parameter, $\mu$, is shown in Fig. 3. Clearly, the nature of the eigenvalues changes at $|\mu/2| = 1$; the normal form Eq. (7) demonstrates a new kind of bifurcation where a pair of eigenvalues transform from pure real to pure imaginary. In the following section, we carry out this analysis in more detail and augment it by drawing the phase portrait of the system.

The final aim is to link the dynamics on the phase plane with the mechanistic understanding of wave interaction presented in the introduction.

## III. DYNAMICAL SYSTEM ANALYSIS

### A. Dynamics on a compact non-Hamiltonian degenerated phase plane

We can express Eq. (7) in terms of $(\chi, \epsilon)$ to obtain the following autonomous, nonlinear dynamical system:

$$\frac{d\chi}{d\tau} = (1 - \chi^2)\sin\epsilon, \quad (13a)$$

$$\frac{d\epsilon}{d\tau} = (\chi + \chi^{-1})\cos\epsilon - \mu. \quad (13b)$$

We note that the (scaled) waves' amplitude ratio and phase difference are, respectively, within the ranges of $\chi \in (0, \infty)$ and $\epsilon \in [-\pi, \pi]$. Equations (13a)–(13b) are in polar coordinates, with $\chi$ being the radius and $\epsilon$ being the azimuthal angle. Equivalently it can be expressed in a Cartesian form:

$$\mathcal{U} \equiv \frac{dX}{d\tau} = Y(\mu - 2X), \quad (14a)$$

$$\mathcal{V} \equiv \frac{dY}{d\tau} = -\mu X + X^2 - Y^2 + 1 \quad (14b)$$

(where $X = \chi\cos\epsilon$ and $Y = \chi\sin\epsilon$), from which we compute the divergence and curl of the phase plane flow:

$$\mathcal{D} \equiv \frac{\partial\mathcal{U}}{\partial X} + \frac{\partial\mathcal{V}}{\partial Y} = -4Y, \quad (15a)$$

$$\mathcal{C} \equiv \frac{\partial\mathcal{V}}{\partial X} - \frac{\partial\mathcal{U}}{\partial Y} = -2(\mu - 2X). \quad (15b)$$

The phase portrait corresponding along with the divergence field and the same along with the curl field are, respectively, shown in Figs. 4 and 5. The fixed points in polar coordinates are

$$(\chi, \epsilon)^* = \left(1, \pm\cos^{-1}\left[\frac{\mu}{2}\right]\right) \text{ when } \left|\frac{\mu}{2}\right| \leqslant 1, \quad (16a)$$

$$(\chi, \epsilon)^* = \left(\frac{\mu}{2} \pm \sqrt{\left[\frac{\mu}{2}\right]^2 - 1}, 0\right) \text{ when } \frac{\mu}{2} \geqslant 1, \quad (16b)$$

$$(\chi, \epsilon)^* = \left(-\frac{\mu}{2} \pm \sqrt{\left[\frac{\mu}{2}\right]^2 - 1}, \pi\right) \text{ when } \frac{\mu}{2} \leqslant -1, \quad (16c)$$

or equivalently in Cartesian coordinates:

$$(X, Y)^* = \left(\frac{\mu}{2}, \pm\sqrt{1 - \left[\frac{\mu}{2}\right]^2}\right) \text{ when } \left|\frac{\mu}{2}\right| \leqslant 1, \quad (17a)$$

$$(X, Y)^* = \left(\frac{\mu}{2} \pm \sqrt{\left[\frac{\mu}{2}\right]^2 - 1}, 0\right) \text{ when } \left|\frac{\mu}{2}\right| \geqslant 1. \quad (17b)$$

The stability of the fixed points is obtained from the eigenvalues, $\lambda_{1,2}^J$, of the Jacobian matrix $J$, evaluated at the fixed points,

$$\frac{d}{d\tau}\begin{bmatrix} \delta X \\ \delta Y \end{bmatrix} = \frac{1}{2}\begin{bmatrix} \mathcal{D} & -\mathcal{C} \\ \mathcal{C} & \mathcal{D} \end{bmatrix}^* \begin{bmatrix} \delta X \\ \delta Y \end{bmatrix}, \quad (18)$$
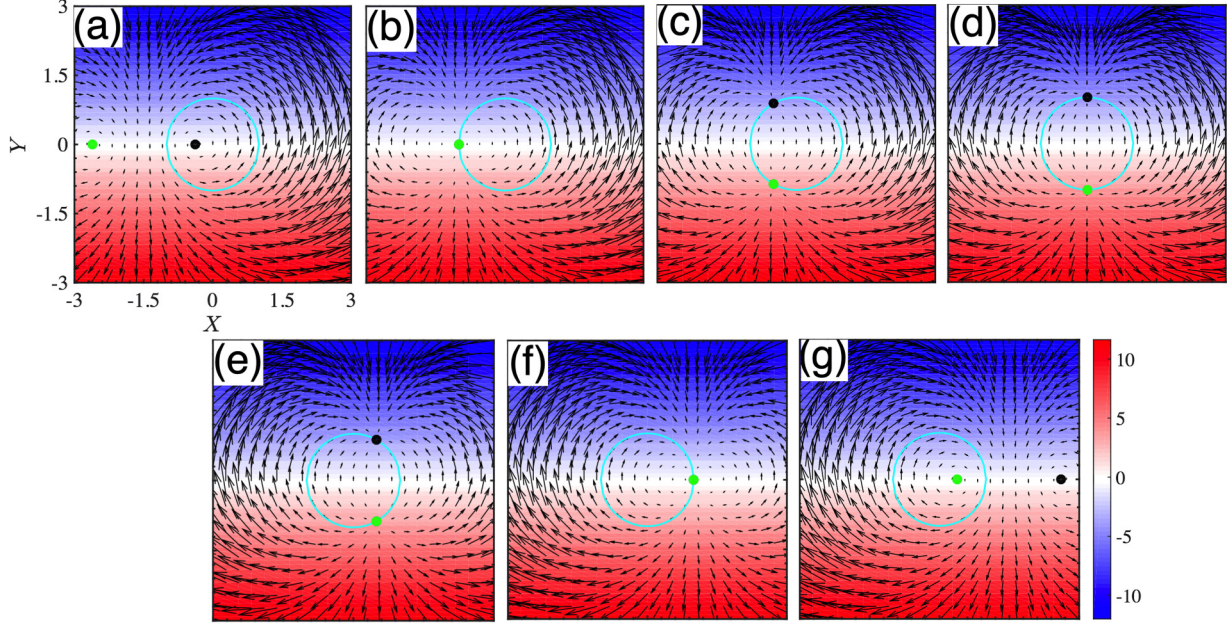
FIG. 4. Phase portrait with colors indicating the divergence field, $\mathcal{D}$. The green and black dots denote the fixed points. A unit circle, centered at the origin, is plotted in cyan. (a) $\mu = -3$, (b) $\mu = -2$, (c) $\mu = -1$, (d) $\mu = 0$, (e) $\mu = 1$, (f) $\mu = 2$, and (g) $\mu = 3$.

yielding $\lambda_{1,2}^J = (\mathcal{D}^* \pm i\mathcal{C}^*)/2$. Transforming $(\delta X, \delta Y) = \delta R(\cos\theta, \sin\theta)$ to polar coordinates whose origin is located at the fixed points, we obtain at the fixed points' vicinity

$$\delta R = \delta R_0 e^{\mathcal{D}^*\tau/2}, \quad \delta\theta = \delta\theta_0 + \mathcal{C}^*\tau/2. \quad (19)$$

### 1. The case of $|\frac{\mu}{2}| < 1$

The control parameter $\mu$ represents the ratio between the difference between the waves' frequencies (in the absence of interaction) and the mean interaction coefficient. The former

acts to shear the waves apart, whereas the latter acts to keep them together.

When $|\mu/2| < 1$, this ratio is not very large, and the obtained fixed points are located on the unit circle ($\chi = 1$), see Eq. (16a). We first note that on the unit circle, the total wave action $\mathcal{A}$ given in Eq. (2b) vanishes. Furthermore, at the fixed points, when in addition $\cos\epsilon = \mu/2$, the pseudoenergy, given in Eq. (2a), vanishes as well. This allows normal mode exponential growth ($\lambda_r^{NM} > 0$) or decay ($\lambda_r^{NM} < 0$) since then these two constants of motion remain zero despite the temporal change in the waves' amplitudes. In order to see that,
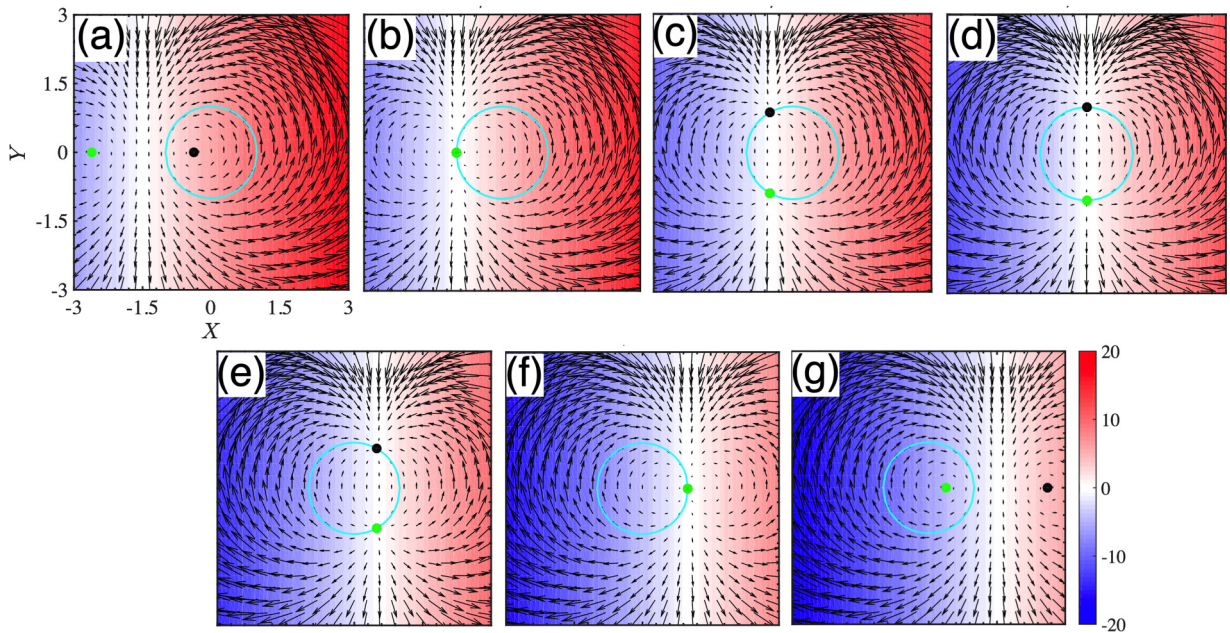


FIG. 5. Phase portrait with colors indicating the curl field, $\mathcal{C}$. Everything else is the same as in Fig. 4.

substitute Eq. (11) in Eqs. (2a)–(2b) to obtain

$$
\mathcal{H} = \left[ -\hat{\omega}_1 \frac{P_1^2}{2\sigma_1} + \hat{\omega}_2 \frac{P_2^2}{2\sigma_2} + \frac{\mu}{2} P_1 P_2 \right] e^{2\lambda_r t},
$$

$$
\mathcal{A} = \left( \frac{P_1^2}{2\sigma_1} - \frac{P_2^2}{2\sigma_2} \right) e^{2\lambda_r t}.
$$

Therefore both $(\mathcal{H}, \mathcal{A})$ must vanish to remain constant when $\lambda_r \neq 0$). On the unit circle, the equation set (13a)–(13b) reduces to

$$
\frac{d\epsilon}{d\tilde{\tau}} = \cos \epsilon - \frac{\mu}{2}, \tag{20}
$$

where $\tilde{\tau} = 2\tau$. Comparing with the synchronization model of Kuramoto [12], here on the right-hand side, we have cosine of the phase difference rather than its sine. This is because the nature of the wave interaction is fundamentally different from the one described in the Kuramoto model. As discussed in Sec. I and specifically in Fig. 2, each wave does not try to adjust its frequency to the other to obtain synchronization. In contrast, when they are in phase, they act to increase their phase difference [see Fig. 2(a)], and when they are in quadrature ($\pi/2$ out of phase), the phase difference is not affected at all by the wave interaction; see Fig. 2(c).

Furthermore, since $\epsilon^* = \pm \cos^{-1}(\mu/2)$, it implies that the fixed points are symmetric with respect to $\epsilon = 0$ (this translates to a reflection symmetry about the $X$ axis in Figs. 4 and 5). Consulting Fig. 2, growth is obtained when $0 < \epsilon < \pi$ (upper half-plane of Figs. 4 and 5) and decay when $-\pi < \epsilon < 0$ (lower half plane). When $\mu = 0$, the waves propagate in concert in the absence of interaction. Hence the only way to keep them locked in the presence of interaction is to prevent the interaction to affect the waves' phase speeds. Thus, the waves' phase difference is either $\pi/2$ [for amplitude growth; Fig. 2(c)] or $-\pi/2$ [for amplitude decay, Fig. 2(d)]. For positive $\mu$, the waves should help each other to counterpropagate in order to remain phase-locked ($-\pi/2 < \epsilon < \pi/2$). In contrast, when $\mu$ is negative, the waves should hinder their counterpropagation rate ($\pi/2 < \epsilon < 3\pi/2$).

The unstable (stable) normal modes are obtained when the amplitude of the two waves grow (decay) with the same exponential growth (decay) rate $\lambda_r^{NM}$. Indeed, as indicated from Eqs. (1a) and (12), for $\chi^* = 1$,

$$
\lambda_r^{NM} = \frac{1}{\sigma} \frac{\dot{Q}_1}{Q_1} = \frac{1}{\sigma} \frac{\dot{Q}_2}{Q_2} = \sin \epsilon^*, \tag{21}
$$

which is positive (negative) for the upper (lower) part of the inner circle in Fig. 2(e). Furthermore, in the frame of reference moving with the mean frequency $\overline{\omega}$, Eq. (12) also yields

$$
\lambda_i^{NM} = \frac{(\dot{\epsilon}_1)^*}{\sigma} = \frac{(\dot{\epsilon}_2)^*}{\sigma} = 0; \tag{22}
$$

hence for $|\mu/2| < 1$, we obtain pairs of growing and decaying normal modes. We can now relate these normal mode stability properties of the physical system with the fixed point stability of the dynamical system on the phase plane. Equations (15)–(17) indicate that for $|\mu/2| < 1$, we have $\mathcal{D}^* = -4 \sin \epsilon^*$, $\mathcal{C}^* = 0$, $\lambda_1^J = \lambda_2^J = \mathcal{D}^*/2 = -2\lambda_r^{NM}$. Hence, both of the fixed points are star nodes, where the physical growing normal mode is a dynamical sink and the decaying mode is a source

in the phase plane. This apparent contradiction actually makes sense when recalling that the physical solution is the superposition of the two normal modes in Eq. (9). Therefore, any initial condition which combines projection on the two normal modes will converge in time to the unstable normal mode as the stable mode decays with time.

### 2. The case of $|\frac{\mu}{2}| > 1$

When $\mu$ exceeds the absolute value of 2, the ratio between the difference between the waves' frequencies (in the absence of interaction) and the mean interaction coefficient becomes too large to allow modal growth. When $\mu > 2$ the shear is too strong, so the waves must be in phase ($\epsilon^* = 0$) to fully help each other to counterpropagate against the shear. In contrast, when $\mu < -2$ the shear is too weak so the waves must be antiphased ($\epsilon^* = \pi$) to fully hinder each other's counterpropagation rate. In both cases Eq. (1a) indicates that amplitude growth is prevented. Furthermore as $|\mu| > 2$, the amplitude symmetry between the waves is broken ($\chi^* \neq 1$), since $(\chi + \chi^{-1})^* > 2$ [cf. Eq. (13b)], where the wave with the larger amplitude affects the other more than vice versa.

Hence for $\mu > 2$, and when $\chi > 1$, the upper wave, with the larger amplitude, will successfully help the lower one to counterpropagate against its mean flow to end up with a positive frequency relative to $\overline{\omega}$ (rightward propagation). On the other hand, the help provided by the lower wave (with the smaller amplitude) to the upper one is less effective, and as a result, the ability of the upper wave to counterpropagate against the rightward mean flow becomes smaller. As a result the upper wave is ending up as well with a positive frequency relative to $\overline{\omega}$. This is how phase locking is achieved for such neutral modes. Reversing the argument when $\chi < 1$ we end up with leftward phase-locked propagation. Following the same logic for $\mu < 2$, and recalling that now the waves hinder each others' propagation, we end up with modal leftward propagation for $\chi > 1$ and rightward for $\chi < 1$. These corresponding compromised frequencies, relative to $\overline{\omega}$, are obtained from the modal eigenvalues (12), where $\omega^* = -\lambda_i^{NM} = \pm \sqrt{\left(\frac{\mu}{2}\right)^2 - 1}$.

Since in this regime the vorticity amplitudes ($Q_{1,2}$) of the waves remain small, these neutral modes have generally little relevance for shear instability. Nevertheless, they are interesting from the dynamical perspective. The vertical line, $X = \mu/2$, in the phase plane is an attractor for $Y > 0$ and a repeller for $Y < 0$. When $|\mu/2| < 1$, the fixed points are located on the intersection between this vertical line and the unit circle, where the stable star node (black dot in Fig. 5) sits on the attracting side and the unstable one (green dot in Fig. 5) on the separating side. When $|\mu/2| > 1$ the two fixed points sit on the $X$ axis at equal distances from the two sides of $X = \mu/2$, where one point is inside the unit circle and the other is outside of it. As is evident from Eqs. (15), (17), and (19), these points are counterrotating center points ($\lambda_{1,2}^J = \pm i |\chi^* - 1/\chi^*|$, $\mathcal{D}^* = 0$, $\mathcal{C}^* = \pm 2\sqrt{\left(\frac{\mu}{2}\right)^2 - 1}$). Hence, when $|\mu/2| = 1$, the normal form of Eq. (7) exhibits bifurcation from a pair of a stable and unstable star nodes to two counterrotating neutral center fixed points; see Fig. 6. We are not familiar with other examples of such a type of bifurcation.
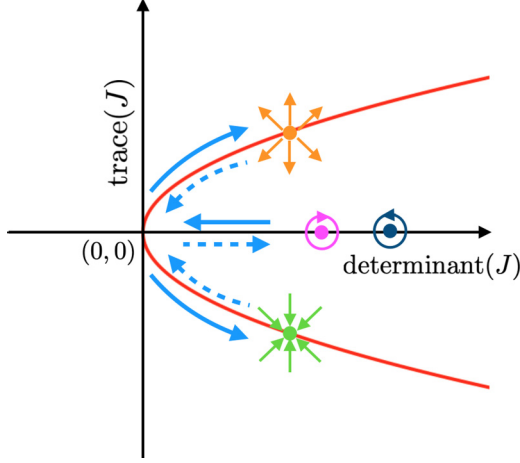
FIG. 6. Trace-determinant diagram of the Jacobian matrix evaluated at the fixed points. Two neutral center fixed points, respectively shown by dark blue (positive circulation) and magenta (negative circulation) circles, approach the origin (path shown by the blue solid arrow) along the determinant axis (where $\mathcal{D}^* = 0$), as the bifurcation parameter, $\mu$, is decreased from a high absolute value to 2 (cf. Fig. 3). A new type of bifurcation occurs at $|\mu| = 2$; as $|\mu|$ is further decreased, a source (filled orange circle with outward arrows) and sink (filled green circle with inward arrows) fixed points are born. These fixed points lie on the trace-determinant parabola (trace$^2 = 4$ determinant where $\mathcal{C}^* = 0$). The exactly opposite behavior happens when $|\mu|$ is increased beyond 2, along the path indicated by the dashed blue arrows.

It is interesting to understand the dynamics of these center modes. Perturbing the phase difference $\epsilon$ from the fully helping or the fully hindering setup immediately yields either a small growth or decay of the wave amplitudes. Since their amplitudes are not even, this growth or decay is more pronounced on the wave with the smaller amplitude, because the wave with the larger amplitude affects the one with the smaller amplitude more efficiently. Thus the amplitude ratio tends to return to its unperturbed value. Similarly, initially changing the amplitude ratio will unlock the waves, and as a result, it changes the amplitude ratio, which will in turn act to restore the phase to its neutral position. Hence, near the fixed points, the system exhibits simple harmonic oscillations. To see this mathematically let us write Eq. (18) in terms of $(\chi, \epsilon)$:

$$\frac{d}{d\tau}\begin{bmatrix} \delta\chi \\ \delta\epsilon \end{bmatrix} = \begin{bmatrix} -2\chi\sin\epsilon & (1-\chi^2)\cos\epsilon \\ (1-\chi^{-2})\cos\epsilon & -(\chi+\chi^{-1})\sin\epsilon \end{bmatrix}^* \begin{bmatrix} \delta\chi \\ \delta\epsilon \end{bmatrix}.$$
(23)

In the vicinity of the neutral fixed points we obtain

$$\frac{d}{d\tau}\delta\chi = \pm(1-\chi^2)^*\delta\epsilon, \quad (24a)$$

$$\frac{d}{d\tau}\delta\epsilon = \pm(1-\chi^{-2})^*\delta\chi, \quad (24b)$$

where the plus (minus) sign corresponds to the case where $\mu$ is larger (smaller) than 2. For either case Eq. (24) yields

$$\frac{1}{\delta\chi}\frac{d^2}{d\tau^2}\delta\chi = \frac{1}{\delta\epsilon}\frac{d^2}{d\tau^2}\delta\epsilon = -[(\chi-\chi^{-1})^2]^* = -(\lambda_i^J)^2,$$
(25)

where $|\lambda_i^J|$ is the oscillation frequency, as expected.

## B. A 3D conservative phase space

The four-equation set (1), or equivalently the Hamiltonian system (3) of the two waves' action-angle conjugate pairs, were mapped in the previous subsection into the two-equation set (13) or equivalently into Eq. (14). Hence, a four degrees of freedom Hamiltonian system was mapped into a degenerate non-Hamiltonian system with only two degrees of freedom. In the former, the fixed points are centers, representing solutions in which the two waves are both neutral and stationary. In the latter, area is not conserved in the phase plane, which allows sink and source fixed points to represent modal growth and decay, respectively. The reason that such mapping is at all possible is that the nonlinear system Eq. (1) emanates from the linearized system Eq. (4), which can be determined only up to an arbitrary complex scaling factor between $q_1$ and $q_2$. The degeneracy results from the fact that the amplitude of such a scaling factor is "hidden" inside $\chi$ and its phase inside $\epsilon$.

Between the (impractical for demonstration) Hamiltonian four-dimensional configuration phase space and the compact nonconservative phase plane we note that the Hamiltonian $\mathcal{H}$ is a function of $A_1$, $A_2$, and $\epsilon$, and not separately of $\epsilon_1$ and $\epsilon_2$; see Eq. (2a). This allows the construction of a three-dimensional (3D) volume-preserving phase space out of these variables. The dynamical equations on this phase space are given by Eq. (3a) (two equations) and the subtraction of the two equations ($\dot{\epsilon}_1$ from $\dot{\epsilon}_2$) of Eq. (3b), yielding

$$\dot{\epsilon} = -\hat{\omega} + i\sigma\left(\sqrt{\frac{\mathcal{A}_2}{\mathcal{A}_1}} - \sqrt{\frac{\mathcal{A}_1}{\mathcal{A}_2}}\right)\cos\epsilon = \frac{\partial\mathcal{H}}{\partial\mathcal{A}_1} - \frac{\partial\mathcal{H}}{\partial\mathcal{A}_2}. \quad (26)$$

Volume is then conserved in this $A_1$-$A_2$-$\epsilon$ phase space:

$$\frac{\partial\dot{\mathcal{A}}_1}{\partial\mathcal{A}_1} + \frac{\partial\dot{\mathcal{A}}_2}{\partial\mathcal{A}_2} + \frac{\partial\dot{\epsilon}}{\partial\epsilon} = 0,$$

as can be easily proved using the facts that

$$\dot{\mathcal{A}}_{1,2} = -\frac{\partial\mathcal{H}}{\partial\epsilon_{1,2}} \quad \text{and} \quad \frac{\partial\epsilon}{\partial\epsilon_1} = 1 \quad \text{and} \quad \frac{\partial\epsilon}{\partial\epsilon_2} = -1.$$

In this phase space the stable and unstable star nodes Eq. (16a) of the 2D phase space are mapped into the lines satisfying $\mathcal{A}_1 = -\mathcal{A}_2$ at the level of $\epsilon^* = \pm\cos^{-1}(\mu/2)$; see Fig. 7(a). The neutral center fixed points of Eqs. (16b)–(16c) are obtained for the lines

$$\mathcal{A}_1 = -\left[\frac{\mu^2}{2} - 1 \pm \mu\sqrt{\left(\frac{\mu}{2}\right)^2 - 1}\right]\mathcal{A}_2,$$

on the surfaces $\epsilon^* = 0$ and $\pi$, respectively, as can be understood from Figs. 7(b)–7(c).

## IV. APPLICATION TO THE RAYLEIGH MODEL OF SHEAR INSTABILITY

We wish to provide a concrete example for the wave interaction mechanism. One of the simplest setups for shear instability was suggested by Lord Rayleigh in 1879 [19] for a
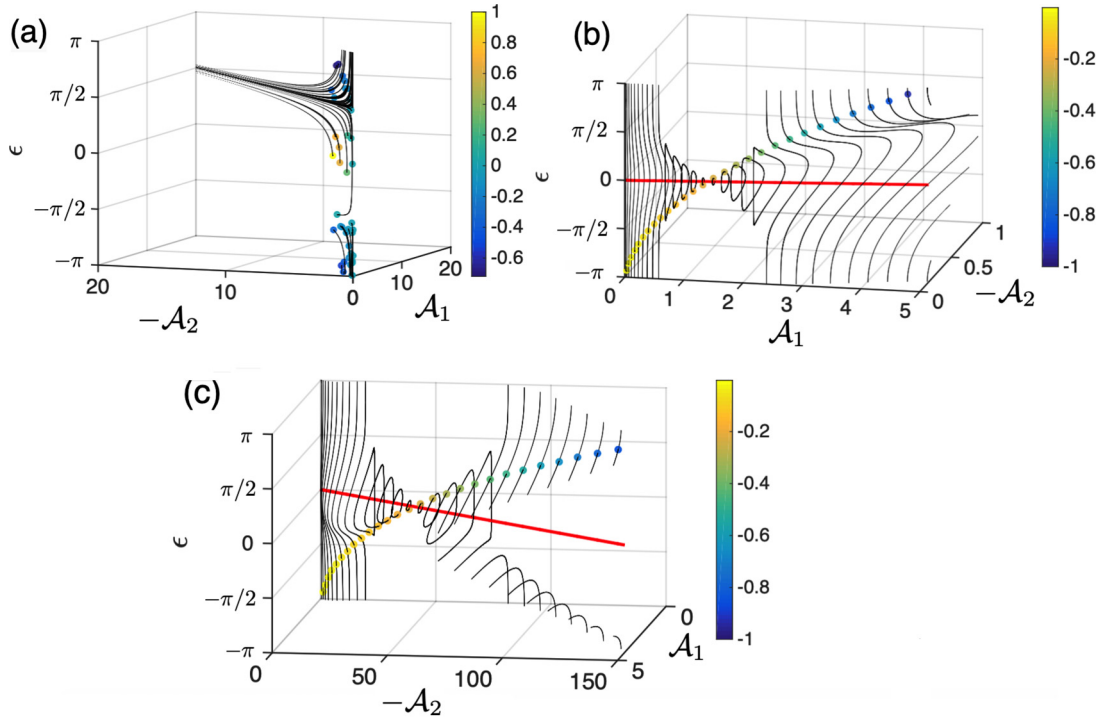
FIG. 7. Phase portrait showing selected trajectories in the conservative phase space $\mathcal{A}_1$-$\mathcal{A}_2$-$\epsilon$. The Rayleigh instability problem of Sec. IV has been chosen. (a) Unstable case: $\mu = 0$ and initial points located along $\mathcal{A}_1 = -\mathcal{A}_2$, (b) Stable case: $\mu = 3$ and initial points located along $\mathcal{A}_1 = -[\mu^2/2 - 1 + \mu\sqrt{(\mu/2)^2 - 1}]\mathcal{A}_2$ and (c) stable case: $\mu = 3$ and initial points located along $\mathcal{A}_1 = -[\mu^2/2 - 1 - \mu\sqrt{(\mu/2)^2 - 1}]\mathcal{A}_2$. The red lines denote $\mathcal{A}_1 = -[\mu^2/2 - 1 + \pm\mu\sqrt{(\mu/2)^2 - 1}]\mathcal{A}_2$ for $\epsilon = 0$. Colors show the normalized pseudoenergy, which, being a constant of motion, remains constant along each trajectory.

piecewise version of the shear profile in Fig. 1:

$$U(y) = \begin{cases} 1 & y \geqslant 1 \\ y & -1 \leqslant y \leqslant 1 \\ -1 & y \leqslant -1 \end{cases}. \tag{27}$$

Detailed analysis of the problem in terms of wave interaction can be found in Ref. [2] for modal instability and in Ref. [20] for nonmodal growth. Here we note that for this piecewise version of shear profile the mean vorticity gradient is concentrated in $y = \pm 1$:

$$\frac{d\Omega}{dy} = -\frac{d^2U}{dy^2} = \delta(y - 1) - \delta(y + 1). \tag{28}$$

Thus the two vorticity waves are interfacial so that the perturbation vorticity $q$ satisfies

$$q = [q_1(k, t)\delta(y - 1) + q_2(k, t)\delta(y + 1)]e^{ikx}, \tag{29}$$

where $k > 0$ denotes the streamwise wave number. Analysis of this symmetric setup reveals that $\sigma = \sigma_1 = \sigma_2 = e^{-2k}/2$ and $\hat{\omega}_1 = -\hat{\omega}_2 = k - 1/2$, yielding $\overline{\omega} = 0$ and $\mu/2 = (2k - 1)e^{2k}$. Hence, the wave number is the actual control parameter of the problem which is mapped into the control parameter $\mu$ of the normal form of Eq. (7). Since $k$ is positive, $\mu/2 > -1$, therefore $k = 0$ is the limit of two infinitely fast counterpropagating waves that must be in antiphase to fully hinder each other's propagation rate in order to remain phase-locked. Furthermore, $k = 0.5$ corresponds to $\mu = 0$ where waves are either $\pi/2$ or $-\pi/2$ out of phase for the growing and decaying

modes, respectively. Since $\mu/2$ becomes larger than 1 for $k_c > 0.64$, it therefore implies that for wave numbers larger than $k_c$, all normal modes are neural. In this scenario, the waves are in phase to fully help each other to counterpropagate against the shear; however, the wave amplitudes are not even. The bifurcation diagram for Rayleigh's shear instability is given in Fig. 8.

## V. MULTIWAVE INTERACTIONS

The interaction between the two vorticity waves, described in Eq. (1), can be generalized straightforwardly to the case of $N$ number of interacting waves, as is illustrated schematically in Fig. 9 and explained in the Appendix of Ref. [21] for Rossby waves and in Ref. [18] for gravity waves. Multiple vorticity waves are located in concave and convex regions where the mean cross-stream vorticity derivative have local extrema. The cross-stream velocity field at every level is now composed of the *in situ* velocity field, induced by the wave located at that level (indicated hereafter by the index $i$, and the contributions of the far field velocity induced by all of the other remote waves, indicated generally by the index $j$). Naturally, the magnitude of the induced velocity decreases with the distance according to the evanescent structure of the Green function, which translates the vorticity source to the far-field velocity field it induces. This structure is determined by the details of the problem setup (cf. different examples in the Appendix of Ref. [20]); however, it depends only on the cross-stream distance between waves $i$ and $j$. In the following
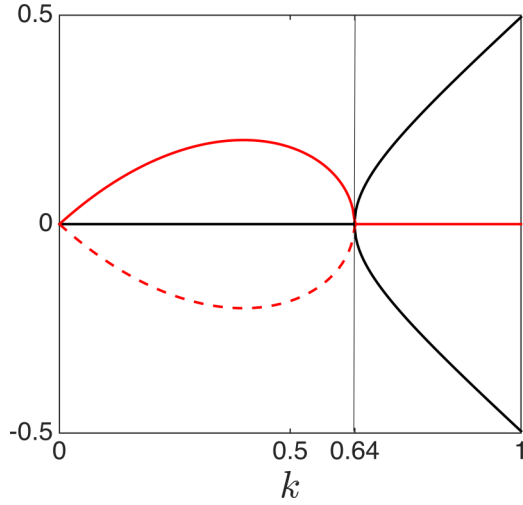
FIG. 8. Bifurcation diagram for Rayleigh instability. Black line denotes $\lambda_i$, solid red line denotes $\lambda_r > 0$, marking the unstable normal mode, and the dashed red line denotes $\lambda_r < 0$, i.e., the stable normal mode. Bifurcation occurs when $k = 0.64$ (shown by the thin vertical line). Direct comparison can be made with Fig. 3, noting that here $\mu$ is always greater than $-2$.

formulation $G_{ij}$ represents the Green function induced by a remote wave $j$ on an *in situ* wave $i$. Since only the distance between the two waves matters for $G$, it is symmetric, i.e., $G_{ij} = G_{ji}$. Generally we may expect that adjacent pairs of vorticity waves will affect each other more pronouncedly than remote pairs. Nonetheless, a remote vorticity wave with a large amplitude $Q_j$ may affect a distant wave more strongly than a closer neighbor wave with a smaller amplitude.

Furthermore, as illustrated in Figs. 1 and 9 the cross-stream velocity field acts directly on the wave displacement. Thus, if the displacement and the vorticity wave anomalies are in phase (like in wave "2" in Fig. 1) a positive far field

cross-stream velocity, acting to amplify the wave displacement, is also amplifying the positive vorticity anomaly. In contrast, when the wave displacement and vorticity anomalies are in antiphase (as in wave "1" in Fig. 1) such far-field velocity will increase the negative value of the vorticity anomaly. The amount by which an induced velocity increases the vorticity amplitude of an *in situ* wave depends on the restoring mechanism of the wave itself and is generally different for Rossby, gravity, capillary, or Alfvén waves. As we are interested in the prototype of the interaction we therefore indicate this factor by $\alpha_i$, which is positive when the displacement and the vorticity wave anomalies of wave $i$ are in antiphase and negative when they are in phase. Denoting $\epsilon_{ij} \equiv \epsilon_i - \epsilon_j$, and $\sigma_{ij} \equiv \alpha_i G_{ij}$, the generalization of Eq. (1) to $N$ interaction waves read

$$\dot{Q}_i = \sum_{j=1}^{N} \sigma_{ij} Q_j \sin \epsilon_{ij}, \tag{30a}$$

$$\dot{\epsilon}_i = -\hat{\omega}_i + \sum_{j=1, j \neq i}^{N} \sigma_{ij} \frac{Q_j}{Q_i} \cos \epsilon_{ij}. \tag{30b}$$

Thus, from this wave interaction perspective modal phase locking is achieved when a configuration is set to synchronize all waves to propagate with the same frequency: $-\omega^* = \lambda_i^{NM} = \dot{\epsilon}_1 = \dot{\epsilon}_2 = \cdots = \dot{\epsilon}_N$, and to exhibit the same growth rate $\lambda_r^{NM} = \dot{Q}_1/Q_1 = \dot{Q}_2/Q_2 = \cdots = \dot{Q}_N/Q_N$.

The wave action and the pseudoenergy conservation laws for Eq. (30),

$$\mathcal{A} = \sum_{i=1}^{N} \mathcal{A}_i = \sum_{i=1}^{N} \frac{Q_i^2}{2\sigma_i}, \quad \mathcal{H} = \sum_{i=1}^{N} \mathcal{A}_i \dot{\epsilon}_i, \tag{31}$$

satisfy then the Hamilton equations

$$\dot{\mathcal{A}}_i = -\frac{\partial \mathcal{H}}{\partial \epsilon_i}, \quad \dot{\epsilon}_i = \frac{\partial \mathcal{H}}{\partial \mathcal{A}_i}. \tag{32}$$
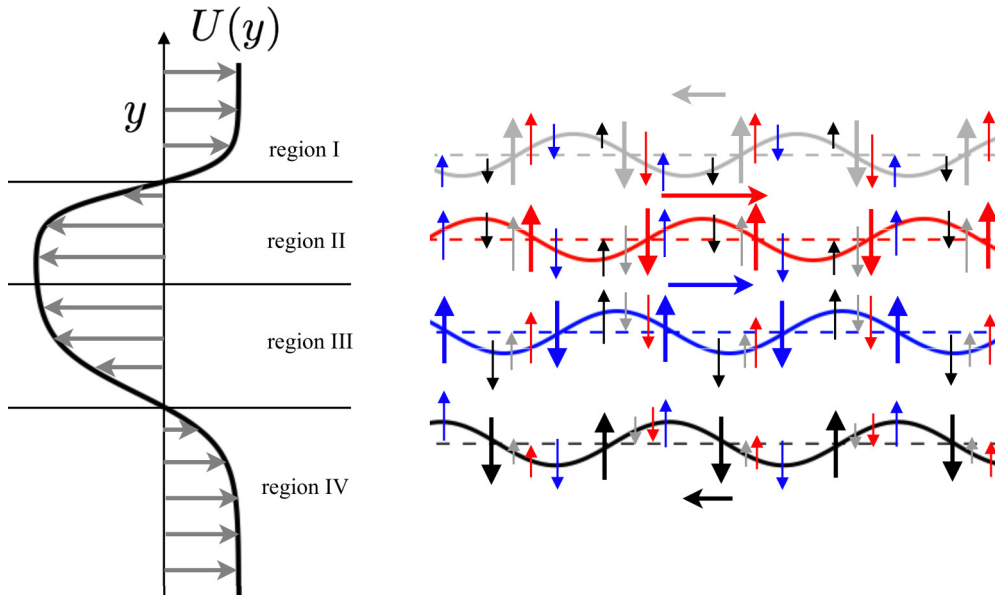


FIG. 9. Schematic of a general shear layer, the complex instability dynamics of which can be understood using the minimal model of $N$ ($= 4$ in this case) interacting vorticity waves. The color convention is same as that of Fig. 1.
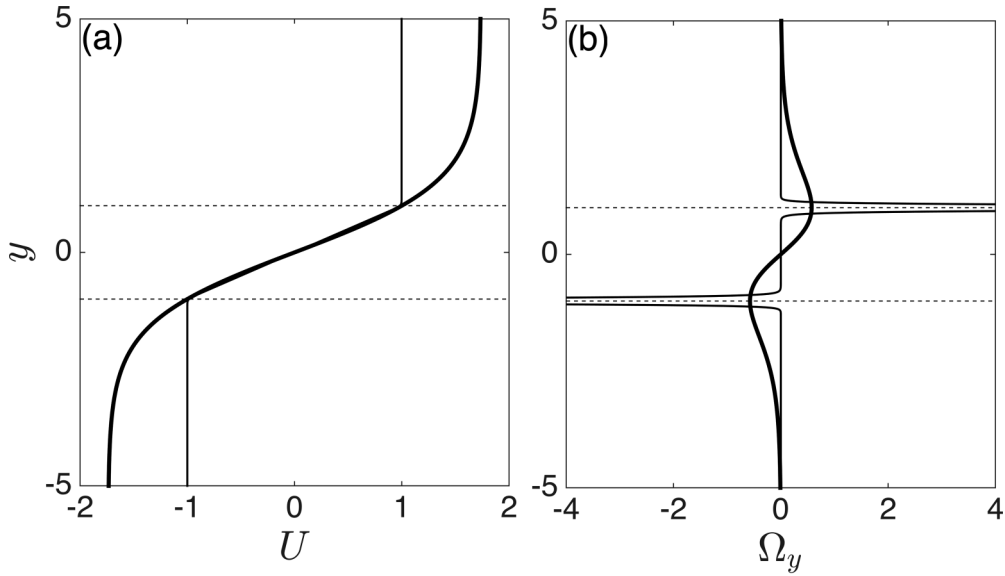
FIG. 10. Rayleigh's piecewise shear layer (thin solid line) and scaled shear layer, $U = \tanh(by)/\tanh(b)$ (thick solid line). The upper (lower) dashed line represents $y = 1(-1)$. (a) Mean velocity profiles and (b) mean vorticity gradient profiles.

## VI. CONCLUSIONS

In this paper we have examined a simple, nonlinear, autonomous dynamical system which describes some central aspects of 2D shear instability. The building blocks of the system are interacting counterpropagating vorticity waves. Instability is achieved when the waves are synchronized to propagate in a phase-locked configuration which allows mutual amplification, i.e., resonance. While this system is a "minimal toy model" it manages to catches the essential mechanism of the instability in different physical setups. The dynamics originates from the linearized vorticity equation for shear flows and therefore is valid only for small wave amplitudes. Hence, triad interactions between waves with different wave numbers are excluded. Nonetheless, the interaction between distant waves of the same wave number across the shear is nonlinear. Mathematically, this nonlinear representation of linearized dynamics results from introducing the perturbation field in its polar form, i.e., in terms of amplitude and phase. However, this apparent additional complication provides a clear mechanistic interpretation for the instability mechanism. A somewhat similar example in which some aspects of linear dynamics become clearer when introduced in its nonlinear polar form is the Madelung equation [22], which converts the linear Schrödinger equation into a fluid dynamic, Euler-like equation [23].

The wave interaction equations are conservative. In the generalized configuration space $\mathbb{R}^{2N}$ (where $N$ is the number of the interacting waves) the pseudoenergy serves as the Hamiltonian, the square of the wave amplitudes are proportional to their wave action, and their phases can be considered as angles. It is then straightforward to show that the system satisfies a generalized action-angle Hamilton equations where the total action of all the waves is conserved; however, the action of each individual wave may change (unlike the classical action-angle formalism) due to the action-at-a-distance interaction between the waves.

Since the wave interaction equations emanate from the linearized dynamics, it is determined up to an arbitrary complex scaling factor between the waves. As a result, the essence of the wave interaction dynamics can be described in a reduced nonconservative phase space with only $N$ degrees of freedom. In this 'reduced' phase space, unstable normal modes of the linearized system are represented by stable star fixed points, and the stable normal modes by unstable star fixed points. This apparent contradiction actually makes sense since in the linearized system, a perturbation solution is a superposition of the unstable (growing) and stable (decaying) normal modes. Hence, as time evolves, the perturbation will be biased towards the unstable normal mode solution, diverging away from the unstable fixed point (in the reduced phase space) and converging towards the stable fixed point. If the shear is either too strong or too weak to allow resonance, synchronization between the waves is still possible. In these scenarios, the waves are phase-locked to propagate in concert with the same frequency; however, the amplitude of the waves does not change due to the interaction between the waves. In the linearized description, these configurations describe neutral normal modes, whereas in the reduced phase space, these are neutral central fixed points.

Furthermore, for the two-wave interaction problem, the dynamics in the reduced phase-space can be succinctly expressed as a complex normal form equation for the normalized perturbation vorticity ratio between the waves. It is a nonhomogeneous equation (since the shear acts as an exterior forcing) which includes a single control parameter. The latter is the ratio between the differences between the waves' frequencies in the absence of interaction and the interaction coefficient. This makes sense as the waves generally tend to propagate in opposite directions in the absence of interaction, whereas the mutual interaction tends to keep them together. This normal form [see Eq. (7)] exhibits bifurcation where annihilation of a pair of stable and unstable star nodes yields

the emergence of two neutral center fixed points of opposite circulations. To the best of our knowledge, this is a new type of bifurcation.

The two-wave and the general $N$-wave interaction dynamics described here can be regarded as well as a novel model for synchronization. Each agent (wave) in isolation acts to resist (counterpropagate against) a local external forcing (the mean flow shear); some agents counterpropagate more efficiently than others. Hence, alignment (phase locking) is achieved only through overall collaboration (far-field interaction) between the agents. The "too efficient" agents should be hindered by the overall interaction whereas the "less efficient" ones should be helped. This dynamics shares some similarities with the Kuramoto model; however, it differs from the latter since here each agent does not try to adjust its frequency to the other to obtain synchronization. In contrast, when the waves are in phase, they act to increase their phase difference.

A further novel aspect of our model is that alignment can lead to mutual amplification of the agents' amplitudes (modal instability). Hence, eventually the agents will be strong enough not only to interact between themselves, but also to alter their "environmental averages" conditions [24], i.e., the mean flow. This is one of the central initial mechanisms by which 2D laminar shear flows are transformed into a turbulent state. A straightforward generalization of such wave–mean flow interaction is currently being studied by the authors.

The interaction described here is a type of long-range interaction. As illustrated in Fig. 9 the instantaneous interaction between each pair of distant waves is not affected by the waves sandwiched in between. However, in reality, for finite values of the Reynolds number, viscosity may play a vital role in the dynamics and should be represented by a short-range interaction [25] between the agents. Another additional piece of reality is that shear flows in nature are generally continuously exposed to some level of noise (both exterior and interior due to triad interaction processes), which affects the mean flow and the waves. Diffusive [25] and stochastic [26] processes have already been implemented in collective dynamics in different contexts and in nonlinear dynamical systems. While wave–mean flow models already exist [27], there remains a considerable scope towards understanding it from the wave interactions perspective. In the near future, the authors aim to provide a more realistic description of counterpropagating wave–mean flow interactions as a forced-dissipative system.

## APPENDIX: EXTENSION OF WAVE INTERACTION THEORY IN RAYLEIGH'S PIECEWISE SHEAR LAYER TO A CONTINUOUS SHEAR LAYER PROFILE

### 1. Derivation of the multilayered equations

Here we show how Rayleigh's piecewise shear layer, discussed in Sec. IV, leads to the dynamical system

(1a)–(1b), and furthermore, how a shear layer with $N$ interfaces, discussed in Sec. V, leads to a more generalized dynamical system (30a)–(30b).

We consider an incompressible, inviscid, 2D flow where the perturbation stream function $\psi(x, z, t)$ and the perturbation vorticity $q(x, z, t)$ are related via

$$\nabla^2 \psi = q. \tag{A1}$$

As before, we assume perturbed quantities to be represented by the Fourier ansatz $f = \Re\{\hat{f}(y, t; k)e^{ikx}\}$, where $k$ is wave number and $f$ could be $\psi$, $q$, or $v$ (where $v = \psi_x = ik\psi$ is the perturbation cross-stream velocity). Such ansatzes when substituted in Eq. (A1) yield

$$\left(\frac{d^2}{dy^2} - k^2\right)\hat{\psi} = \hat{q}. \tag{A2}$$

The linear operator in the left-hand side is inverted to yield

$$\hat{\psi} = -\int_{\mathcal{B}} G(y', y; k)\hat{q}(y', t; k)\, dy', \tag{A3}$$

where $\mathcal{B}$ is the domain and $G(y', y; k)$ is the appropriate positive definite Green's function, which also depends on the boundary conditions. We consider an unbounded domain, for which $G = e^{-k|y-y'|}/(2k)$.

The evolution equation of perturbation vorticity under linearization reads

$$\frac{Dq}{Dt} \equiv \frac{\partial q}{\partial t} + U\frac{\partial q}{\partial x} = -v\frac{d\Omega}{dy}. \tag{A4}$$

Substitution of Eq. (A3) in Eq. (A4) yields

$$\frac{\partial q}{\partial t} + ikUq = ik\frac{d\Omega}{dy}\int_{\mathcal{B}} G(y', y; k)q(y', t)\, dy'. \tag{A5}$$

If we assume a system with $N + 1$ layers, each having a constant vorticity, then

$$\frac{d\Omega}{dy} = \sum_{j=1}^{N} \Delta\Omega_j \delta(y - y_j), \tag{A6}$$

where $\Delta\Omega_j \equiv \Omega(y_j^+) - \Omega(y_j^-)$. The discrete spectrum solution of Eq. (A4) is then simply given by

$$q = \sum_{j=1}^{N} q_j(t)\delta(y - y_j)e^{ikx}, \tag{A7}$$

$$\psi = -\frac{1}{2k}\sum_{j=1}^{N} q_j(t)e^{-k|y-y_j|}e^{ikx}. \tag{A8}$$

On expressing $q_j(t) = Q_j(t)e^{i\epsilon_j(t)}$, substitution of Eq. (A7) in Eq. (A5) yields

$$\dot{Q}_i = \frac{\Delta\Omega_i}{2}\sum_{j=1}^{N} Q_j e^{-k|y_i-y_j|}\sin\epsilon_{ij}, \tag{A9a}$$

$$\dot{\epsilon}_i = -\hat{\omega}_i + \frac{\Delta\Omega_i}{2Q_i}\sum_{j=1, j\neq i}^{N} Q_j e^{-k|y_i-y_j|}\cos\epsilon_{ij}, \tag{A9b}$$

where $\epsilon_{ij} \equiv \epsilon_i - \epsilon_j$ and $\hat{\omega}_i = kU_i - \Delta\Omega_i/2$. Equations (A9a)–(A9b), signifying Rossby wave interactions in a general shear layer shown in Fig. 9, are a special case of
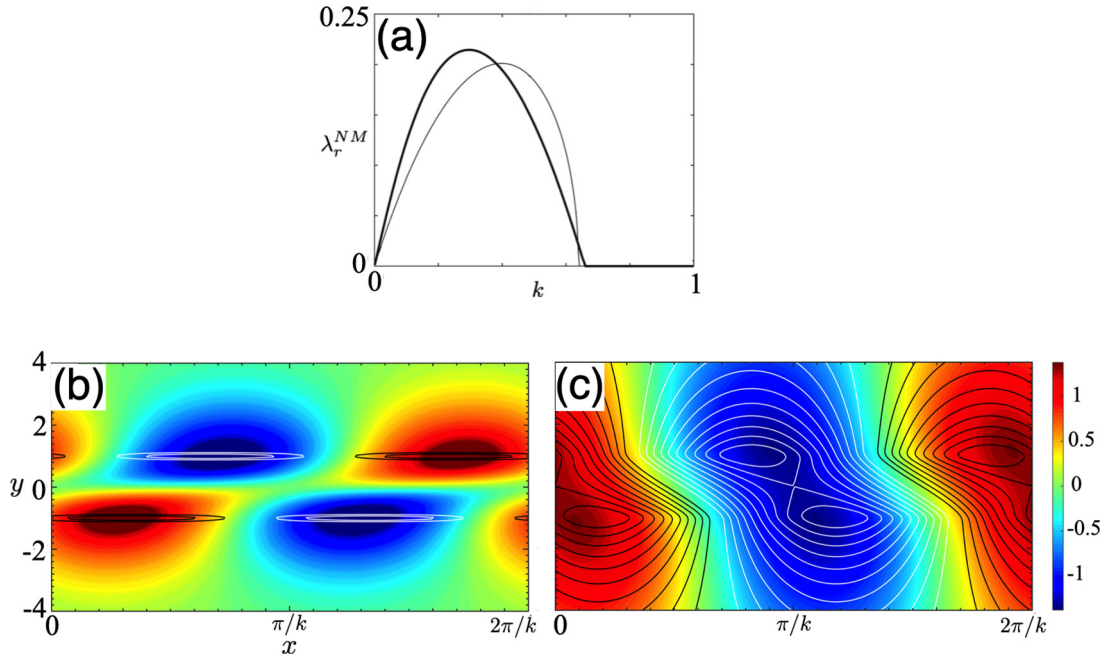
FIG. 11. (a) Dispersion relation, i.e., growth rate versus wave number for Rayleigh (gray) and scaled hyperbolic tangent shear layer (black). (b) Normalized perturbation vorticity for Rayleigh (black and white contour lines; black denotes positive and white denotes negative) and scaled hyperbolic tangent shear layer (filled colored contours). (c) Normalized perturbation streamfunction following the same color scheme as in panel (b).

Eqs. (30a)–(30b). Furthermore, Eqs. (A9a)–(A9b) can be straightforwardly applied to Rayleigh's shear layer problem discussed in Sec. IV by taking $N = 2$ and the correct $\Delta\Omega_i$ values (i.e., that of Rayleigh's shear layer).

### 2. Comparison of instabilities in piecewise and continuous shear layers

Rayleigh's shear layer profile, discussed in Sec. IV, is shown in Fig. 10 with a thin solid line. It is assumed to be an approximation of the more realistic, hyperbolic tangent shear layer. While Rayleigh's profile can be understood using two-wave interactions, the hyperbolic tangent shear layer is more complex and requires many (technically infinite) wave interactions. Yet the basic mechanism of wave synchronization and resonance remains the same, as described by Eqs. (A9a)–(A9b). While the unstable region for Rayleigh's profile is $0 < k < 0.64$ [see Fig. 11(a)], the same for the hyperbolic tangent shear layer, i.e., $U = \tanh(y)$ is $0 < k < 1$ (not shown in the figure, but see Drazin and Reid [19]). This discrepancy is mainly due to an improper scaling, as discussed in Carpenter *et al.* [9]. The extrema of the base vorticity gradient for the shear layer $U = \tanh(by)/\tanh(b)$ peaks at $y = \pm 1$ (shown in Fig. 10 by thick solid lines), where $b = 0.66$, unlike that

of $U = \tanh(y)$, which peaks at $y = \pm 0.66$ (not shown in the figure). Additionally, the shear profile $U = \tanh(by)/\tanh(b)$ attains $U(\pm 1) = \pm 1$. Hence the Rayleigh's piecewise shear layer profile is expected to provide a far more accurate comparison with $U = \tanh(by)/\tanh(b)$ than with $U = \tanh(y)$.

For any $k$, the normal mode growth rate, $\lambda_r^{NM}$ of a shear layer can be obtained via standard eigenvalue analysis. In Fig. 11(a) we compare the dispersion relation of the two profiles in question and observe a very good match. In Fig. 11(b) we compare the vorticity perturbations of the unstable modes corresponding to $k = 0.38$ of the two profiles. For this value of $k$, the scaled smooth shear layer and Rayleigh's shear layer have the same growth rate. In Rayleigh's profile, the perturbation vorticity is localized at $y = \pm 1$, as expected for $\delta$ functions (unlike the smooth shear layer, which is more spread out). However, the perturbation stream functions obtained by inverting the corresponding perturbation vorticities are quite similar, as is evident from Fig. 11(c). Moreover, the phase difference $\epsilon^*$ for these two profiles is in good agreement and has a value of $\approx 0.6\pi$. This conclusively shows that Rayleigh's profile, where phase locking of two Rossby waves provides an accurate description of the instability mechanism, provides a very good minimal model description of the smooth shear layer.

[1] B. J. Hoskins, M. E. McIntyre, and A. W. Robertson, On the use and significance of isentropic potential vorticity maps, Q. J. Roy. Meteor. Soc. **111**, 877 (1985).

[2] E. Heifetz, C. H. Bishop, and P. Alpert, Counter-propagating Rossby waves in the barotropic Rayleigh model of shear instability, Q. J. Roy. Meteor. Soc. **125**, 2835 (1999).

[3] L. Rayleigh, On the stability, or instability, of certain fluid motions, Proc. Lond. Math. Soc. **1**(1), 57 (1879).

[4] H. C. Davies and C. H. Bishop, Eady edge waves and rapid development, J. Atmos. Sci. **51**, 1930 (1994).

[5] E. T. Eady, Long waves and cyclone waves, Tellus **1**, 33 (1949).

[6] J. Methven, B. J. Hoskins, E. Heifetz, and C. H. Bishop, The counter-propagating Rossby-wave perspective on baroclinic instability. Part IV: Nonlinear life cycles, Q. J. Roy. Meteor. Soc. **131**, 1425 (2005).

[7] N. Harnik, E. Heifetz, O. M. Umurhan, and F. Lott, A buoyancy-vorticity wave interaction approach to stratified shear flow, J. Atmos. Sci. **65**, 2615 (2008).

[8] A. Guha and G. A. Lawrence, A wave interaction approach to studying non-modal homogeneous and stratified shear instabilities, J. Fluid Mech. **755**, 336 (2014).

[9] J. R. Carpenter, E. W. Tedford, E. Heifetz, and G. A. Lawrence, Instability in stratified shear flow: Review of a physical interpretation based on interacting waves, Appl. Mech. Rev. **64**, 060801 (2013).

[10] L. Biancofiore, F. Gallaire, and E. Heifetz, Interaction between counterpropagating Rossby waves and capillary waves in planar shear flows, Phys. Fluids **27**, 044104 (2015).

[11] E. Heifetz, J. Mak, J. Nycander, and O. M. Umurhan, Interacting vorticity waves as an instability mechanism for magnetohydrodynamic shear instabilities, J. Fluid Mech. **767**, 199 (2015).

[12] A. Pikovsky, M. G. Rosenblum, and J. Kurths, *Synchronization, A Universal Concept in Nonlinear Sciences* (Cambridge University Press, Cambridge, 2001).

[13] I. S. Aranson and L. Kramer, The world of the complex Ginzburg-Landau equation, Rev. Mod. Phys. **74**, 99 (2002).

[14] R. Fjørtoft, On the changes in the spectral distribution of kinetic energy for two-dimensional, nondivergent flow, Tellus **5**, 225 (1953).

[15] E. Heifetz, C. Bishop, B. Hoskins, and J. Methven, The counter-propagating Rossby-wave perspective on baroclinic instability. I: Mathematical basis, Q. J. Roy. Meteor. Soc. **130**, 211 (2004).

[16] Note that in Fig. 2, the displacement fields have been plotted. In Fig. 2(a) the displacement fields are antiphased; however, the vorticity fields are in phase.

[17] N. Harnik, D. G. Dritschel, and E. Heifetz, On the equilibration of asymmetric barotropic instability, Q. J. Roy. Meteor. Soc. **140**, 2444 (2014).

[18] E. Heifetz and A. Guha, A generalized action-angle representation of wave interaction in stratified shear flows, J. Fluid Mech. **834**, 220 (2018).

[19] P. G. Drazin and W. H. Reid, *Hydrodynamic Stability*, 2nd ed. (Cambridge University Press, Cambridge, 2004).

[20] E. Heifetz and J. Methven, Relating optimal growth to counter-propagating Rossby waves in shear instability, Phys. Fluids **17**, 064107 (2005).

[21] E. Heifetz, N. Harnik, and T. Tamarin, Canonical Hamiltonian representation of pseudoenergy in shear flows using counter-propagating Rossby waves, Q. J. Roy. Meteor. Soc. **135**, 2161 (2009).

[22] E. Madelung, Quantentheorie in hydrodynamischer Form, Z. Phys. A **40**, 322 (1927).

[23] E. Heifetz and E. Cohen, Toward a thermo-hydrodynamic like description of Schrödinger equation via the Madelung formulation and Fisher information, Found. Phys. **45**, 1514 (2015).

[24] S. Motsch and E. Tadmor, Heterophilious dynamics enhances consensus, SIAM Rev. **56**, 577 (2014).

[25] R. Shvydkoy and E. Tadmor, Topological models for emergent dynamics with short-range interactions, arXiv:1806.01371 (2018).

[26] B. Düring, P. Markowich, J.-F. Pietschmann, and M.-T. Wolfram, Boltzmann and Fokker–Planck equations modelling opinion formation in the presence of strong leaders, Proc. Royal Soc. A **465**, 3687 (2009).

[27] J. Pedlosky, *Geophysical Fluid Dynamics*, 2nd ed. (Springer-Verlag, New York, 1990), p. 710.